Cavity configurations for soft-aperture Kerr-lens mode locking and multiple-period bifurcations in Ti:sapphire lasers

Ja-Hon Lin, Ming-Dar Wei, and Wen-Feng Hsieh*

Institute of Electro-Optical Engineering, National Chiao Tung University, 1001 Tahsueh Road, Hsinchu 30050, Taiwan

Hsiao-Hua Wu

Department of Physics, Tunghai University, 181 Section 3 Chung Kang Road, Taichung 407, Taiwan

Received November 7, 2000; revised manuscript received March 12, 2001

We find that soft-aperture Kerr-lens mode locking (SAKLM) in a Ti:sapphire laser always takes place around certain discrete cavity configurations accompanied by peculiar beam patterns. By correlating the superposition of proper transverse modes to the observed beam patterns and fitting the beat frequencies to the resonance equation, we discovered that the patterns for SAKLM are formed by phase locking of the fundamental mode with specific degenerate transverse modes that occur near different degenerate cavity configurations. As predicted by the stability analysis, period-3 and period-2 SAKLM does occur around the 1/3- and 1/4-degenerate cavity configurations, which cannot be fully explained in terms of total mode locking of TEM_{00} and TEM_{01} modes. © 2001 Optical Society of America

OCIS codes: 140.4050, 190.3270, 140.3410, 140.1540, 140.3580.

1. INTRODUCTION

Since the first demonstration of self-mode locking[1] in a Ti:sapphire laser, a great deal of effort has been made in both theory[2–7] and experiments[1,3,8–11] to search for the conditions for generating ultrashort optical pulses with stable operation and the ability to self-start. The basic mechanism underlying pulse formation in the Ti:sapphire laser is attributed to Kerr-nonlinearity-induced self-focusing to modulate the cavity loss or gain, which is referred to as hard-aperture[1,3,8] or soft-aperture[9,10,11] Kerr-lens mode locking (KLM), respectively. Although the calculated Kerr-lens mode-locked strength is insufficient to self-start KLM of a Ti:sapphire laser,[2] self-starting a hard-aperture Kerr-lens mode-locked (HAKLM) laser has been accomplished near the edge of the stability region, where the laser has the largest hard-aperture Kerr-lens mode-locked strength.[8] Moreover, the observed region for self-starting hard-aperture Kerr-lens mode-locked operation agrees well with the previous stability analysis based on minimizing the Hamiltonian as a function of spot size and curvature of the cavity and use of the intracavity power as an adjusting parameter for various cavity configurations.[12]

By analyzing the iterative map of Gaussian-beam propagation in a general optical resonator, we predicted that the transverse-mode degenerate[13] cavity configurations that correspond to the so-called low-order resonance[14,15] may become unstable under persisting nonlinear effects.[15,16] Juang *et al.*[10] showed that the soft-aperture Kerr-lens mode-locked (SAKLM) laser has maximal saturated differential gain near the center of the least-misalignment-sensitive (LMS) stable region,[3] where the cavity-configuration-dependent power dip is observed. Power dips and specific mode patterns have also been observed in a diode-pumped Nd:YVO_4 laser with a simple two-mirror resonator around various degenerate cavity configurations.[17,18]

In this paper we report the specific cavity configurations suitable for the SAKLM operation in a Ti:sapphire laser. By examining the cavity-configuration-dependent output of the Ti:sapphire laser, we observed several power dips with specific beam patterns existing around certain discrete cavity configurations within the LMS stable region. Using the transverse-mode beating measured near confocal configurations to fit the resonance equation, we verify that these power dips occur near different degenerate cavity configurations. To know what modes these peculiar beam patterns contain and to quantitatively confirm the fractions of constitutive transverse modes, we correlate the superposition of some selected cavity modes to the measured beam patterns. The results indicate that the SAKLM patterns could be decomposed into those low-order degenerate transverse modes along with the fundamental one.

Moreover, we observed period-3 KLM occurring around the 1/3-degenerate configuration.[13] From the spatial correlation of the experimental and reconstructed beam patterns we find that the period-3 SAKLM pattern contains the TEM_{01} mode, which can be explained by the total mode locking.[19] Nevertheless, unlike the results reported previously that period-2 KLM occurred at an effective confocal cavity,[20] we found the period-2 KLM taking place around the 1/4-degenerate configuration ($G_1G_2 = 1/2$), which can be explained by the total mode locking

0740-3224/2001/081069-07$15.00

only if the TEM_{02} mode is involved instead of the TEM_{01} mode. The existence of the TEM_{02} mode in period-2 SAKLM pulsing was confirmed by correlating the superposition of proper transverse modes to the observed beam patterns. In our previous prediction[15] based on the residue theorem the period-2 and period-3 mode locking may be generated at $G_1G_2 = 1/2$ and 1/4, resulting from the nonlinear-dynamics-induced spot-size variation.

This paper is organized as follows: In Section 2 we describe our experimental setup used for the study of the SAKLM laser. The cavity configuration suitable for the SAKLM laser and their identification are described in Section 3. The spatial correlation of the measured beam patterns with the superposition of degenerate transverse modes is accounted for in Section 4. The period-2 and period-3 KLM are explicitly discussed in Section 5 to study what mechanism is responsible. Finally, conclusions are drawn in Section 6.

2. EXPERIMENTS

Our experimental setup is shown in Fig. 1, which is a standard astigmatically compensated z-folded four-mirror cavity containing a 9-mm-long Brewster-cut Ti:sapphire rod. Two spherical mirrors M_1 (pump side) and M_2, both with a 10-cm radius of curvature, were highly reflecting over the 770–870-nm spectral range and highly transmitting for the 488–532-nm pump wavelength. The distance from the curved mirror M_1 to one end surface of the laser rod is denoted as r_1 and from the other end surface to another curved mirror M_2 as r_2. Two flat mirrors, a 98% high reflector M_4 and a 95% output coupler M_5, were placed to form linear arms with M_2 at a distance of d_1 and M_1 at a distance of d_2, respectively, in a near-symmetric arrangement. Two Brewster-angled SF-10 glass prisms were inserted between M_1 and M_3 with a distance of ~27 cm for group-velocity dispersion compensation in the femtosecond regime. The total length of the resonator is approximately 160 cm, resulting in an axial mode spacing of 93.3 MHz or a cavity round-trip time of 10.7 ns. An all-line continuous-wave (cw) Ar-ion laser (Coherent, Innova 300) was employed to pump the Ti:sapphire crystal by a plano-convex lens with a focal length of 12.7 cm. The lens, the laser rod, and the folding mirrors were mounted on precision translation stages to allow for fine adjustment of the resonator configuration and the overlap between the pump beam and the cavity mode. The laser beam from the 98% high reflector M_4 was focused on two high-speed photodetectors (Electro-Physics Technology ET-2000), and their outputs were sent to a 300-MHz digital oscilloscope (LeCroy 9450A) and a spectrum analyzer (Hewlett-Packard, 8560E) for monitoring the pulse sequence and the radio-frequency power spectrum, respectively. A CCD camera was used for observing the transverse pattern of the laser beam.

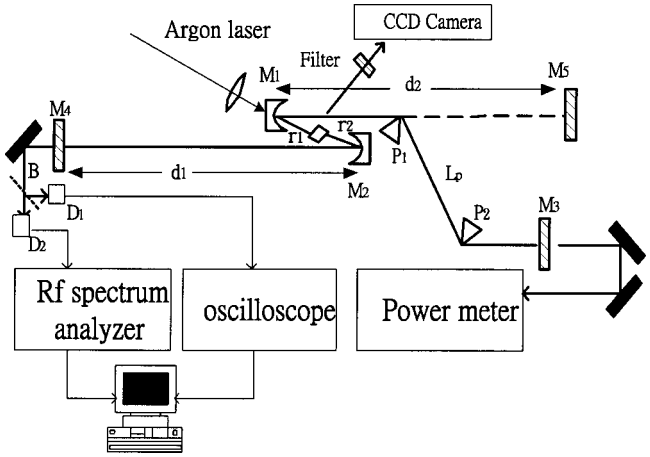

Fig. 1. Experimental setup of the Kerr-lens mode-locking Ti:sapphire laser. D_1 and D_2 are high-speed detectors, and B is beam splitter.

3. CAVITY CONFIGURATIONS FOR SAKLM LASER

To achieve the SAKLM operation, we displaced the folding mirror M_2 along the cavity axis over a geometrically stable region of the resonator. The output average powers and beam profiles were then measured as a function of the M_2 position that corresponds to a certain value of r_2. Generally, the laser could be made to operate in a single TEM_{00} mode apart from some critical M_2 positions in which the decreases in laser power form dips and different peculiar beam patterns that were observed. We found that SAKLM operation always took place near these positions. To determine the dependence of cavity configurations on r_2 with high accuracy, we measure the transverse-mode beat frequencies for different M_2 positions. It is worth mentioning that the transverse-mode beating can be easily observed only when M_2 is positioned close to the effective confocal cavity configuration. Thus we measured five successive beat frequencies and their corresponding M_2 positions. By fitting the beat frequencies with the resonance equation[13] for the transverse-mode spacing ω, $\omega = (\Omega/\pi)\cos^{-1}[(G_1G_2)^{1/2}]$, we are able to obtain the precise cavity configurations specified by G_1G_2 in terms of r_2. Here $\Omega = c/2L$ is the longitudinal-mode spacing, L is the total cavity length, and c is the speed of light in vacuum. From Ref. 14 one obtains $G_1 = a$ and $G_2 = d$ with $\left[\begin{smallmatrix} a & b \\ c & d \end{smallmatrix}\right]$ being the one-way transfer matrix between two flat end mirrors M_4 and M_5. We can relate the one-way transfer matrix to the cavity parameters as

$$a = \frac{(d_2 - f_{\text{eff}})\delta}{f_{\text{eff}}^2} - 1,$$

$$b = a(d_1 + 1) + (d_2 - 2f_{\text{eff}}) + 1,$$

$$c = \frac{\delta}{f_{\text{eff}}^2},$$

$$d = \frac{(d_1 - f_{\text{eff}})\delta}{f_{\text{eff}}^2} - 1.$$

Here $\delta = (L_{\text{eff}} + r_1 + r_2 - 2f_{\text{eff}})$ is defined as the stability parameter;[4] in addition, the effective focal lengths f_{eff} and the effective optical length L_{eff} of the gain medium are given by $f/\cos\theta$ and L/n_0 for the saggital direction and $f\cos\theta$ and $L/{n_0}^3$ in the tangential direction.[5] The condition for $\omega/\Omega = n_t/n_l$, where n_t and n_l are integers, is re-

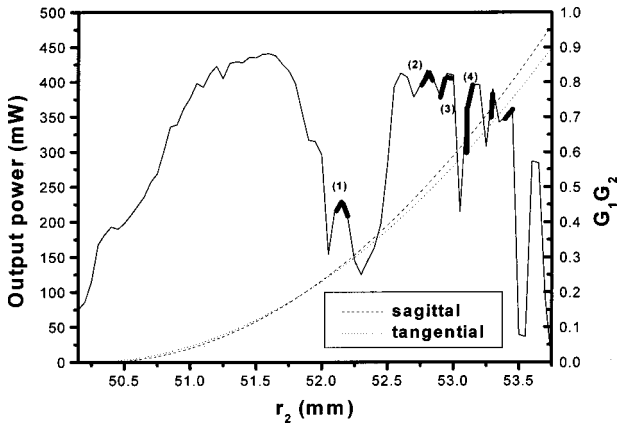

Fig. 2. Measured output power (solid curve) and G_1G_2 for the sagittal (dash) and tangential (dotted) planes as a function of r_2 in the LMS region. The thick parts of the solid curve label the mode-locking region at each degenerate configuration.

ferred to as the transverse-mode degeneracy corresponding to the n_t/n_l degenerate cavity configuration. At this specific configuration the resonant frequency of TEM_{qmn} modes coincide with the $\mathrm{TEM}_{(q+nl)00}$ modes, where q is the longitudinal-mode index, m and n are transverse-mode indices, and $m + n = n_t$.[13]

Figure 2 shows the measured result of output power (solid curve) and G_1G_2 for the sagittal (dash) and tangential planes (dotted) as a function of r_2 in the LMS region. The figure shows that the LMS region extends over 3.6 mm, corresponding to r_2 being changed from 50.15 to 53.75 mm. The power dips are located at (1) $G_1G_2 = 1/4$ with $\omega/\Omega = 1/3$, (2) $G_1G_2 = 1/2$ for the sagittal plane with $\omega/\Omega = 1/4$, (3) $G_1G_2 = 1/2$ for the tangential plane with $\omega/\Omega = 1/4$, and (4) $G_1G_2 = 0.6545$ for the sagittal plane with $\omega/\Omega = 1/5$, respectively. Both the second and the third power dips occur at the configurations for $G_1G_2 = 1/2$ with one on the sagittal plane and the other on the tangential plane. Thick curves label the SAKLM regions that correspond to different degenerate cavity configurations.

Similarly, observations of power dips around different degenerate cavity configurations have been reported elsewhere.[10,17,18] In the degenerate cavity configurations the laser is able to self-adjust its cavity field to extract more energy from the gain medium and lower the lasing threshold for a tightly focused axial pump Nd:YVO_4 laser.[17,18] Beam-waist shrinkage in the power-dip region for operation with the multiple-pass transverse mode[14,18] was observed to result from a low threshold with a penalty of low slope efficiency.

4. BEAM PATTERNS FOR SAKLM LASER

The beam patterns observed for both the cw and picosecond KLM operations in the aforementioned SAKLM regions are no longer pure fundamental Gaussian modes, as shown in the left column of Fig. 3. It might be due to the reason that in an axially pumped laser, especially for the SAKLM laser with the pump size less than the cavity beam size, it is easy to excite the higher-order transverse modes to extract more stored energy from the gain medium when the laser is operated in the degenerate cavity configuration.[17,18] To know what transverse modes these output beam patterns contain, we properly add fractions of several high-order Hermite–Gaussian modes with phase shifts relative to the fundamental one; that is, the modulus of the fundamental and the high-order transverse modes are set to 1, α, and β, their corresponding phase shifts to 0, ϕ_α, and ϕ_β, and so on. Although the matched degree of the simulated beam patterns with the measured ones can be visually recognized, we have maxi-

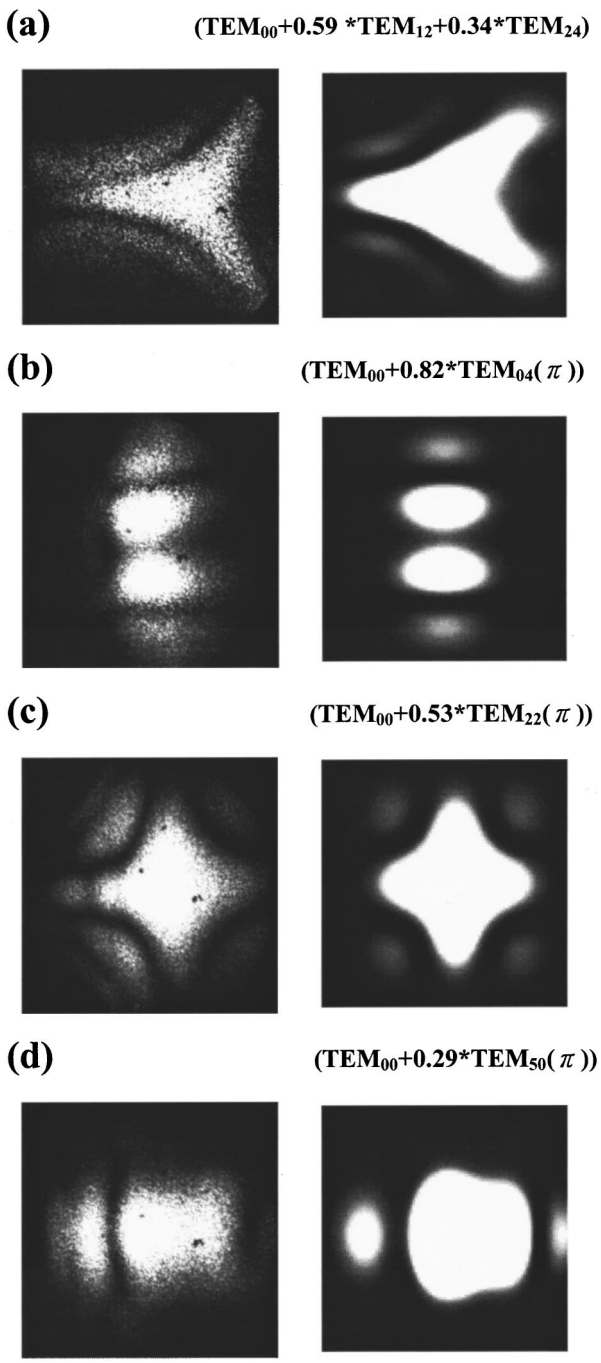

Fig. 3. Measured (left column) and imitated patterns (right column) of the picosecond mode locking at the configuration of (a) $G_1G_2 = 1/4$ (sagittal), (b) $G_1G_2 = 1/2$ (sagittal), (c) $G_1G_2 = 1/2$ (tangential), and (d) $G_1G_2 = 0.6545$ (sagittal). The configurations as well as the amplitude and relative phases of transverse modes are listed atop each figure in the right column.

Table 1. Chosen Transverse Eigenmodes and the Ratio of Radii in the Tangential and Sagittal Directions Used to Simulate the Imitated Beam Patterns of Picosecond ML in Fig. 3 with Their Results Correlated to the Measured Beam Patterns

Pattern	W_t/W_s	Mode	C
A	1.55	(1,2), (2,4)	0.9097
B	1.02	(0.4)	0.9425
C	0.92	(2,2)	0.9291
D	0.96	(5,0)	0.9144

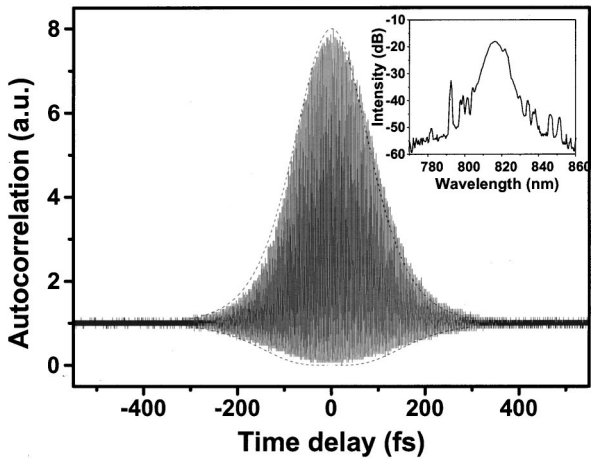

Fig. 4. Typical measured autocorrelation trace (solid curve) and corresponding optical spectrum (right inset) at the state of femtosecond pulses. Note that the dashed curve represents the fitting result by use of the sech^2 function.

mized the correlation coefficient (C) to determine the best-matched patterns with the error within nearly 1%. Accordingly, it allowed the amplitude variations of resembling mode patterns to be less then 0.1 for most of the cases and sometimes even less than 0.05.

To calculate the correlation coefficient, we scaled the simulated beam radii in both the sagittal and the tangential directions as well as translated the beam center to get the best correlation with the measured pattern. However, for correlating the saturated beam patterns we further chose a saturation parameter to simulate the saturated images taken from the CCD. The correlation coefficient is as good as 0.99 for an unsaturated pattern like the one measured from the period-3 KLM (discussed in Section 5) and at least 0.91 for the saturated pattern.

We plotted the matched intensity distributions next to the observed ones (left column) in the right column of Fig. 3. The corresponding parameters including configurations, amplitudes, and relative phases of transverse modes are listed atop the simulated patterns. Note that to obtain similar mode patterns, one needs at least one of the high-order degenerated transverse modes with the relative phase of either 0 or π plus the fundamental mode. In Fig. 3(a) the beam pattern for the 1/3-degenerate ($G_1G_2 = 1/4$) configuration is composed of $0.59\mathrm{TEM}_{12} + 0.34\mathrm{TEM}_{24}$ in phase with TEM_{00}. Figures 3(b) and 3(c) are both 1/4-degenerate ($G_1G_2 = 1/2$) configurations that are constructed from the combination of $\mathrm{TEM}_{00}+0.82\mathrm{TEM}_{04(\pi)}$ on the sagittal plane and $\mathrm{TEM}_{00} + 0.53\mathrm{TEM}_{22(\pi)}$ on the tangential plane, respectively. Here the subscript π represents the relative phase. The fourth pattern [see Fig. 3(d)] belongs to the 1/5-degenerate configuration that has the TEM_{05} mode with the amplitude of 0.29 and a π-phase shift plus the fundamental mode to best match the observed pattern. Table 1 summarizes the w_t/w_s (the reconstructed mode radii in the tangential and sagittal directions), constituting transverse modes and their corresponding correlation coefficients for all the constructed patterns in Fig. 3. These results indicate that the mode patterns for SAKLM

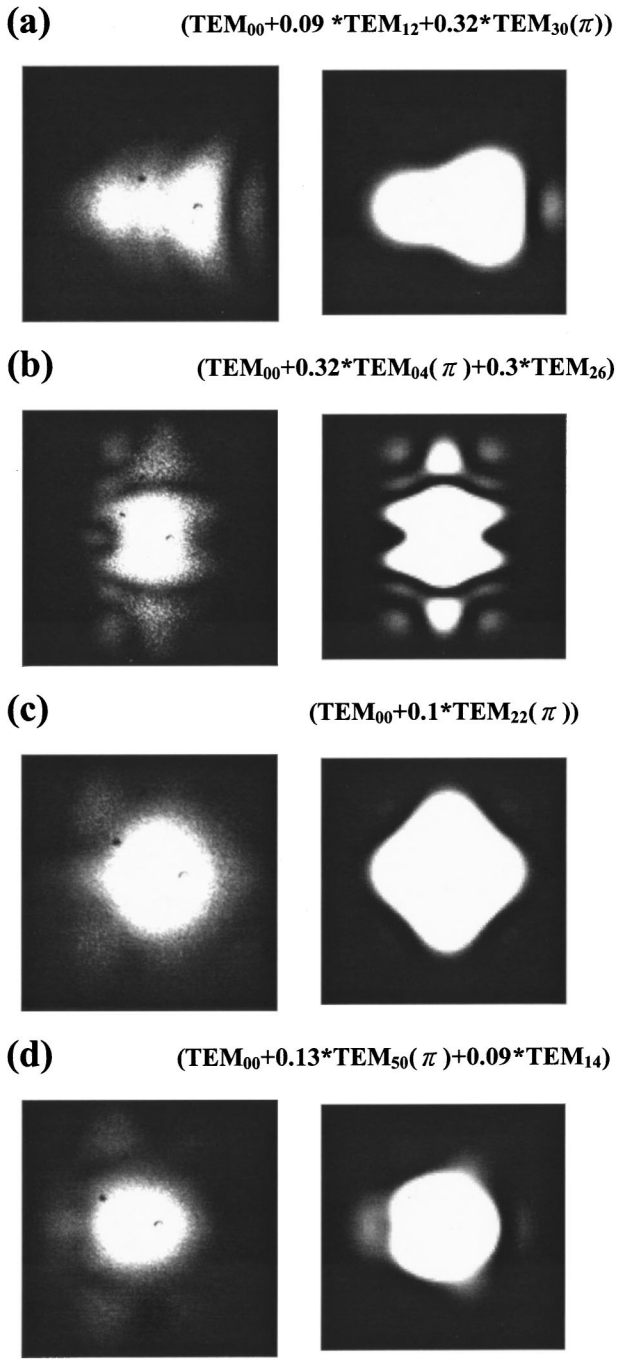

Fig. 5. Measured femtosecond mode locking (left column) and imitated patterns (right column) from the corresponding configurations of Fig. 3.

Table 2. Chosen Transverse Eignmodes and the Ratio of Radii in the Tangential and Sagittal Directions Used to Simulate the Imitated Beam Patterns of Femtosecond ML in Fig. 5 and Periods 2 and 3 with Their Results Correlated to the Measured Beam Patterns

Pattern	W_t/W_s	Mode	C
A	1.37	(1,2), (3,0)	0.9604
B	1.0	(0.4), (2,6)	0.9415
C	1.01	(2,2)	0.9418
D	1.0	(5,0), (1,4)	0.9496
P2	1.08	(0,4)	0.9762
	1.09	(0,4), (0,2)	0.9861
P3	1	(3,0)	0.9656
	1	(3,0), (1,0)	0.9896

operation and in our experiment involve at least one of the low-order transverse modes that degenerate with the fundamental mode.

With insertion of a prism pair in the laser cavity the cw patterns are slightly more complicated than that for the picosecond KLM case, which may be due to collapse of cavity symmetry when the prisms are inserted. We found the femtosecond pulses also at the same configurations, and the self-starting KLM occurs in these regions with a smaller tuning range. A typical interference autocorrelation trace is shown in Fig. 4 that has a pulse width of 110 fs by fitting with the sech^2 function, and its corresponding optical spectrum is also displayed in the inset. While adjusting the insertion of the second prism into the light beam, we can tune the center wavelength of the SAKLM laser from 810 nm to 780 nm with a pulse width in the range 140–60 fs.

Figure 5 shows beam patterns at the corresponding configurations in Fig. 3 with the left column being those patterns for femtosecond mode locking and the right column for imitated ones. The constructed parameters are also listed above each figure. The KLM patterns are smoother and closer to the fundamental ones than the picosecond KLM and cw patterns. To decompose femtosecond mode patterns by linear superposition of the low-order transverse degenerate modes with the fundamental one, we use results that show the ratio of TEM_{12} in Fig. 5(a) decreases to 0.09, and another degenerate mode of TEM_{24} is replaced by the $\text{TEM}_{30(\pi)}$ mode with a proportion of 0.32 as compared with the picosecond case in Fig. 3(a). In addition, reconstruction of the mode pattern of Fig. 5(b) needs an extra 0.3TEM_{26} mode and a lower amplitude of $0.32\text{TEM}_{04(\pi)}$, and $0.13\text{TEM}_{50(\pi)}$ plus 0.09TEM_{14} to imitate Fig. 5(d). Similarly, the ratio of $\text{TEM}_{22(\pi)}$ is also down to 0.1 in Fig. 5(c), which may be partly caused by the fundamental mode having more concentrated energy on the optical axis to extract more stored energy from the gain medium and thus cause larger pattern modulation through self-focusing than the high-order modes do. The other reason might be the phase locking of longitudinal modes, and therefore self-phase modulation broadens the lasing spectrum to decrease temporal coherence and diminish the speckle. The calculated correlation coefficients of reproduced patterns with measured ones of femtosecond pulses as well as period-3 and period-2 (discussed in Section 5) KLM are also summarized in Table 2.

5. PERIOD-3 AND PERIOD-2 KLM

Slightly adjusting the insertion of the prism P2 into the light beam at the configurations $G_1G_2 = 1/4$ and 1/2, we could obtain stable period-3 and period-2 mode-locking pulse trains [Figs. 6(a) and 6(b)]. Figure 7(a) is the three-dimensional intensity-distribution plot of the experimental measured period-3 beam pattern. We followed the aforementioned method using the degenerate TEM_{30} mode (since it is for the 1/3-degenerate configuration) plus the TEM_{00} to imitate the experimental beam pattern. The imitated pattern with the highest correlation coefficient of 0.966 with this experimental beam pattern is shown in Fig. 7(b).

However, we suspected that the period-3 mode locking might be a result of total mode locking.[19] We further added the additional TEM_{10} mode with the successive round-trip phases $\phi_\beta = 0$, $2\pi/3$, and $4\pi/3$ to TEM_{00} and TEM_{30} modes to best correlate the measured one [see Figs. 7(d)–7(f)]. An intensity integration of these three patterns is shown in Fig. 7(c) having $C \approx 0.990$ with the experimental one. In comparison with the correlation results of Figs. 7(b) and 7(c) with Fig. 7(a) the latter showed a better match level by 0.024, which is more than 1% error. Furthermore, we can clearly see a shoulder on the right-hand side of the main bumps in Figs. 7(a) and 7(c) but not in Fig. 7(b). Therefore we believe that the total mode-locking mechanism may be responsible for the period-3 mode locking.

Although the period-2 mode locking has been reported previously in Ti:sapphire laser around the confocal configuration, we found that the period-2 mode locking could also occur at $G_1G_2 = 1/2$, as shown in Fig. 6(b). In this

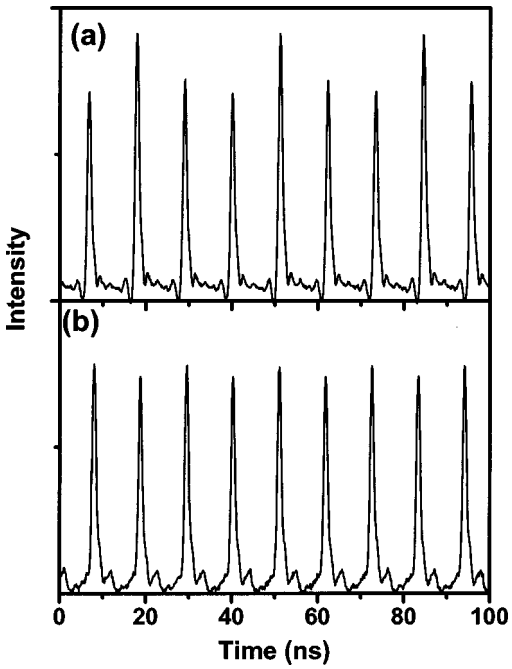

Fig. 6. Pulse train of (a) period-3 and (b) period-2 mode locking.

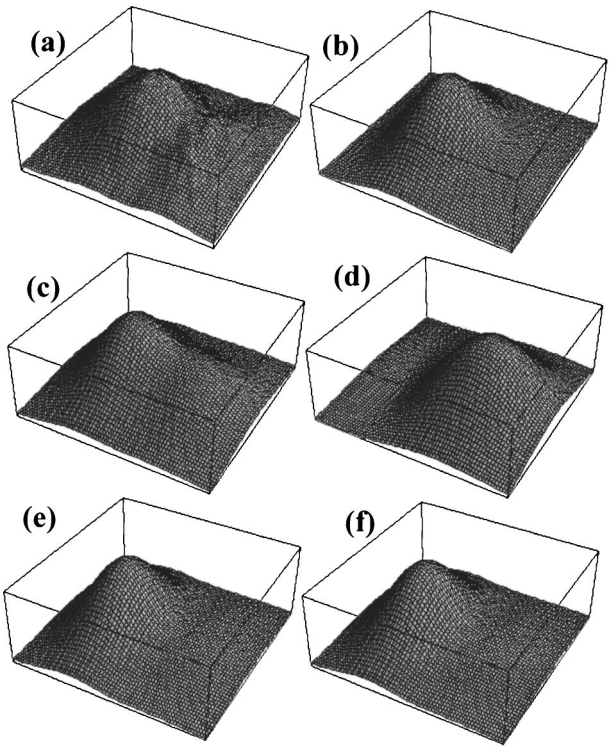

Fig. 7. Intensity distribution of the beam pattern for (a) measured period-3 mode locking, (b) the imitated one by the superposition of the TEM_{00} and TEM_{30}, and (c) the imitated integration of three successive round-trip patterns of superposition of TEM_{00}, TEM_{30}, and TEM_{10} with its relative phase ϕ_β equal to (d) 0, (e) $2\pi/3$ and (f) $4\pi/3$, respectively.

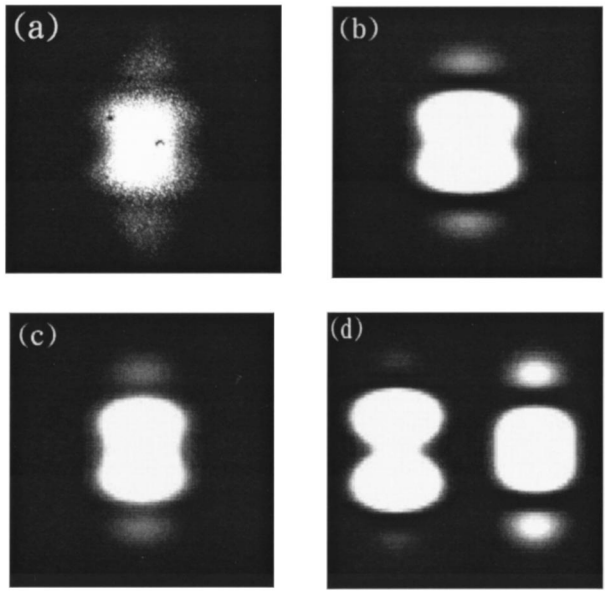

Fig. 8. Beam pattern for (a) the measured period-2 mode locking, (b) the imitated one by the superposition of TEM_{00} and $TEM_{04(\pi)}$, and (c) the imitated integration of two successive round-trip patterns with the superposition of the TEM_{00}, $TEM_{04(\pi)}$, and TEM_{02} with its relative phase ϕ_β equal to 0 (right) and π (left) in (d).

configuration, period-4 mode locking is expected rather than period 2 if the total mode locking by means of the superposition of TEM_{00} and TEM_{10} modes dominated. On the other hand, the period-2 mode locking may be caused by the "breathing"-like periodic spot-size variation of superposition of the degenerate modes in two successive round trips at the 1/4-degenerate configuration that has the second-order resonance.[14,15] With extraction of different stored energies from the gain medium through overlapping of the cavity and axially pumped beams, the output would periodically vary, as predicted by the stability analysis[14,15] considering only Gaussian-beam propagation.

We also used the degenerate transverse modes $TEM_{00}+TEM_{04(\pi)}$ to simulate the measured period-2 beam pattern [Fig. 8(a)]. This imitated pattern [Fig. 8(b)] resembles visually the experimental beam pattern with a correlation coefficient of 0.976. Further including the nondegenerate transverse mode TEM_{02} in successive round trips with relative phases of 0 and π [see Fig. 8(d)], we found the imitated beam pattern [Fig. 8(c)] with a correlation coefficient of 0.986, which shows a better match to the measured one.

It should be noted that the intensity variation in the time trace of the period-3 pulsing is apparent [Fig. 6(a)]; on the contrary, only nearly 5% intensity alternation between two neighboring pulses is observed in Fig. 6(b) at the period-2 mode-locking state. The beam pattern of period-3 mode locking consists of the TEM_{10} mode with the successive phase change, which would cause the intensity distribution to be spatially sweeping [see Figs. 3(d)–3(f)]. As a result, the detected intensity apparently changes when one keeps the position of the high-speed detector fixed at one side of the beam pattern. However, the imitated beam pattern consisting of TEM_{02} with the successive phases of 0 and π in the period-2 case is spatially symmetric so that it brings a smaller change in the detected intensity.

The best correlation results show additional transverse modes with the periodic relative phase shift being the possible cause of multiperiod pulses, which can be explained in terms of the total mode locking. It should be noted that the lower-order transverse mode of TEM_{01} is easier to excite than the TEM_{02} mode in an axially pumped laser. Therefore we expect to observe the period-4 mode locking instead of the period 2 in the 1/4-degenerate configuration if the total mode locking dominated. The stability analysis[14,15] that considers only the Gaussian-beam propagation (w, R) in a general resonator not only provides a good prediction of the cavity configuration at which the subharmonic oscillation will occur, but also other nonlinear dynamics that cannot be directly expressed in terms of linear superposition of cavity eigenmodes.

6. CONCLUSIONS

We have experimentally determined the discrete soft-aperture Kerr-lens mode-locking regions in a Ti:sapphire laser that are located within a series of power dips that correspond to transverse-mode degenerates no matter whether the laser is operated at picosecond or femtosecond mode locking. The self-starting SAKLM operation can also be observed in these regions with a less-tunable range. By spatially correlating the SAKLM beam pat-

terns with the linear superposition of the selected transverse modes, we found that these patterns are attributed to phase locking of the fundamental mode or the lower-order degenerate transverse modes. As predicted by previous stability analysis, we observed the period-3 and period-2 mode locking around the 1/3- and 1/4-degenerate configurations. The best correlation results suggest that additional transverse modes with successive phase shift is a probable reason that the total mode locking seems to apply. The SAKLM laser operated with the 1/4-degenerate configuration at $G_1G_2 = 1/2$, which has been expected to be period 4 by the total mode locking of TEM_{00} and TEM_{01} modes, results in period-2 mode locking. The stability analysis considers only the Gaussian-beam propagation based on *ABCD* law in a general resonator and provides a good prediction of the cavity configuration at which the subharmonic oscillation will occur. This research provides a useful suggestion for cavity design of the soft-aperture Kerr-lens mode-locked laser to generate picosecond and femtosecond pulses and to study its nonlinear dynamics.

ACKNOWLEDGMENTS

This research was partially supported by the National Science Council of the Republic of China under grant NSC89-2112-M-009-037 and NSC87-2112-M-029-002 and 89-E-FA06-1-4 by the Ministry of Education. J.-H. Lin thanks the National Science Council of the Republic of China for providing a fellowship.

*To whom correspondence should be addressed. E-mail: wfhsieh@cc.nctu.edu.tw. Fax: 886-3-5716631.

REFERENCES

1. D. E. Spence, P. N. Kean, and W. Sibbett, "60-fsec pulse generation from a self-mode-locked Ti:sapphire laser," Opt. Lett. **16**, 42–44 (1991).
2. J. Hermann, "Theory of Kerr-lens mode locking: role of self-focusing and radially varying gain," J. Opt. Soc. Am. B **11**, 498–512 (1994).
3. G. Cerullo, S. De Silvestri, V. Magni, and L. Pallaro, "Resonators for Kerr-lens mode-locked femtosecond Ti:sapphire lasers," Opt. Lett. **19**, 807–809 (1994).
4. K.-H. Lin and W.-F. Hsieh, "Analytical design of symmetrical Kerr-lens mode-locking laser cavities," J. Opt. Soc. Am. B **11**, 737–741 (1994).
5. K.-H. Lin, Y. Lai, and W.-F. Hsieh, "Simple analytical method of cavity design for astigmatism-compensated Kerr-lens mode-locked ring lasers and its applications," J. Opt. Soc. Am. B **12**, 468–475 (1995).
6. J. L. A. Chilla and O. E. Martinez, "Spatial-temporal analysis of the self-mode-locked Ti:sapphire," J. Opt. Soc. Am. B **10**, 638–643 (1993).
7. K.-H. Lin and W.-F. Hsieh, "Analytical spatial-temporal design of Kerr lens mode-locked laser resonators," J. Opt. Soc. Am. B **13**, 1786–1793 (1996).
8. G. Cerullo, S. D. Silvestri, and V. Magni, "Self-starting Kerr-lens mode locking of a Ti:sapphire laser," Opt. Lett. **19**, 1040–1042 (1994).
9. M. Lai, "Self-starting, self-mode-locked Ti:sapphire laser," Opt. Lett. **19**, 722–724 (1994).
10. D.-G. Juang, Y.-C. Chen, S.-H. Hsu, K.-H. Lin, and W.-F. Hsieh, "Differential gain and buildup dynamics of self-starting Kerr lens mode-locked Ti:sapphire laser without an internal aperture," J. Opt. Soc. Am. B **14**, 2116–2121 (1997).
11. J.-G. Lai, K.-H. Lin, D.-G. Juang, and W.-F. Hsieh, "Construction of a wavelength-tunable self-starting Kerr lens mode locked Ti:sapphire laser system," Chin. J. Phys. (Taipei) **34**, 111–121 (1996).
12. M.-D. Wei, W.-F. Hsieh, and C. C. Sung, "The preferable resonators for Kerr-lens mode-locking determined by stability factors of their iterative maps," Opt. Commun. **155**, 406–412 (1998).
13. A. E. Siegman, *Lasers* (University Science, Mill Valley, Calif., 1986), Chaps. 20 and 21.
14. M.-D. Wei, W.-F. Hsieh, and C. C. Sung, "Dynamics of an optical resonator determined by its iterative map of beam parameters," Opt. Commun. **146**, 201–207 (1998).
15. M.-D. Wei and W.-F. Hsieh, "Cavity-configuration-dependent nonlinear dynamics in Kerr-lens mode-locked lasers," J. Opt. Soc. Am. B **17**, 1335–1342 (2000).
16. M.-D. Wei and W.-F. Hsieh, "Bifurcation of fundamental Gaussian modes in Kerr-lens mode-locked lasers," Opt. Commun. **168**, 161–166 (1999).
17. H.-H. Wu, C.-C. Sheu, T.-W. Chen, M.-D. Wei, and W.-F. Hsieh, "Observation of power drop and low threshold due to beam waist shrinkage around critical configurations in an end-pumped Nd:YVO_4 laser," Opt. Commun. **165**, 225–229 (1999).
18. H.-H. Wu and W.-F. Hsieh, "Observation of multipass transverse modes in an axially pumped solid state laser with different fractional degenerate resonator configurations," J. Opt. Soc. Am. B **18**, 7–12 (2001).
19. S. R. Bolton, R. A. Jenks, C. N. Elkinton, and G. Sucha, "Pulse-resolved measurements of subharmonic oscillations in a Kerr-lens mode-locked laser," J. Opt. Soc. Am. B **16**, 339–343 (1999).
20. D. Cote and H. M. van Driel, "Period doubling of a femtosecond Ti:sapphire laser by total mode locking," Opt. Lett. **23**, 715–717 (1998).